Spatio-Temporal Kriging for Monthly Precipitation Interpolation in East Kalimantan

Friendtika Miftaqul Jannah[1*], Rahma Fitriani[1], and Henny Pramoedyo[1]
[1]Department of Statistics, Brawijaya University, Malang City, Indonesia
*Corresponding author: friendtika@student.ub.ac.id

Received: 18 December 2024
Revised: 17 April 2025
Accepted: 4 May 2025

ABSTRACT – **Precipitation is one of the factors that can lead to various disasters, such as droughts and floods. Ordinary interpolation methods, such as spatial kriging, cannot accommodate the time element, which is crucial for addressing precipitation-related disasters. Therefore, this study applies a spatio-temporal kriging, which incorporates both spatial and temporal elements. The aim of this study is to develop a spatio-temporal kriging model for precipitation, serving as a basis for interpolating precipitation at unobserved points over various time intervals within the study domain. This model is expected to be an effective tool for disaster mitigation and water conservation strategies. The data used in this study comprises total monthly precipitation recorded at seven precipitation observation posts in East Kalimantan from 2021 to 2023. The findings indicate that the spatio-temporal ordinary kriging model is the most suitable approach, with the best semivariogram model identified as the simple sum-metric. The spatial semivariogram follows an exponential model, while the temporal and joint semivariograms follow Gaussian models. The accuracy of the chosen model yields an RMSE of 2493.687. The interpolation results reveal that West Kutai falls within the medium to high precipitation category, making it the district with the highest flood risk.**

Keywords– **Interpolation, Precipitation, Spatio-Temporal**

I. INTRODUCTION

East Kalimantan has undergone a major transformation with its designation as the relocation site for the National Capital (IKN). This change is expected to have significant environmental impacts. The move of IKN to East Kalimantan is projected to trigger rapid urbanization in several areas, increasing greenhouse gas emissions due to human activities. This will exacerbate climate change, potentially contributing to unstable precipitation patterns and triggering extreme weather. Capturing the high spatiotemporal variability of precipitation is essential in urban environments, where high impermeability leads to rapid runoff generation [1]. Replacing forests and open land with impermeable surfaces such as asphalt and concrete increases stormwater runoff, potentially causing flooding during heavy rains. Deforestation also reduces the soil's ability to absorb water and regulate the natural hydrological cycle, decreasing clean water availability, worsening floods during high precipitation, and heightening drought risks during low precipitation periods [2].

To mitigate these negative environmental impacts, comprehensive environmental planning and sustainable water resources management are essential. High precipitation, which has the potential to cause flooding, requires accurate spatial and temporal estimates to support effective mitigation strategies [3]. Precipitation variability across space and time is crucial to quantify streamflow magnitude and uncertainty properly, which can lead to flooding [4]. Thus, detailed spatio-temporal precipitation information is vital for identifying high-risk flood areas while supporting water resource conservation efforts.

Kriging is a geostatistics prediction method that provides the best linear unbiased predictor (BLUP) [5]. Kriging aims to predict values at unobserved locations based on values at observed locations using a weighted linear combination of the observed locations that minimizes expected squared error derived from a semivariogram [6], [7]. The semivariogram defines the spatial variability of the dependent variable. With advancements in technology and the increasing need for complex analysis, kriging is not only applied to the spatial dimension but also to the temporal dimension. Spatio-temporal kriging is a method that combines spatial and temporal dimensions to provide more accurate predictions for datasets with spatiotemporal dependencies. The spatio-temporal kriging can utilize observations to model spatio-temporal variation and correlation [8].

Applying spatio-temporal kriging to predict precipitation in East Kalimantan is essential to support environmental planning in the region. This model has proven effective in various similar studies, especially in hydrology and climate studies, due to its ability to predict precipitation at unobserved locations and times. Several studies have demonstrated that spatio-temporal kriging produces high-quality interpolation results. A study by Raja found that spatio-temporal kriging can capture precipitation variability patterns effectively, producing smoother and more accurate predictions than conventional spatial-only interpolation methods [9]. Additionally, this method has proven useful in identifying precipitation trends and anomalies, which are crucial for water resource planning and disaster risk management [9]. Similarly, a study by De Carvalho et al. concluded that spatio-temporal kriging successfully provides better estimates of daily precipitation with smaller mean square errors compared to kriging and cokriging [10]. This method exhibits a higher linear correlation between observed data and predictions and less bias than spatial kriging or cokriging. By applying spatio-temporal kriging, it is possible to analyze future precipitation patterns even in unobserved areas, enabling more effective and targeted water conservation and flood mitigation planning.

While these prior studies focused on evaluating the methodological superiority of spatio-temporal kriging in general or in broad hydrometeorological applications, this study distinguishes itself by specifically applying the method in the context of East Kalimantan, a region undergoing unprecedented land use transformation due to the IKN relocation. The spatial and temporal dynamics resulting from massive urban development and deforestation in this region have not been sufficiently explored in existing literature. Therefore, this research not only applies spatio-temporal kriging but also integrates it with the current socio-environmental changes unique to East Kalimantan to generate location-specific precipitation predictions for flood mitigation and water resource planning.

Based on this description, researchers aim to interpolate precipitation in East Kalimantan using the spatio-temporal kriging method. The results of this study are expected to assist local authorities in managing water resources and mitigating flood risks, supporting sustainable development in the region. Moreover, this research may contribute to future studies by enhancing estimation accuracy and spatialization over time.

II. LITERATURE REVIEW

A. Spatio-Temporal Kriging

Spatio-temporal kriging aims to predict unknown point values $Z(s_0, t_0)$ at an unobserved point (s_0, t_0). All available data regarding regional variables are used for this purpose, either at point across the domain or within neighborhoods, which are subsets of the domain. An example $\{\boldsymbol{Z}(\boldsymbol{s}, t), \boldsymbol{s} \in D, t \in T\}$ is given with $D \subseteq \mathbb{R}^2$ and $T \subseteq \mathbb{R}$, being random function spatio-temporal and it is assumed that random area values have been observed in n spatio-temporal data points $\{Z(s_1, t_1), \dots, Z(s_n, t_n)\}$. To predict the value of a random region spatio-temporal at an unobserved point (s_0, t_0), a linear predictor is used in equation (1) [11].

$$\hat{Z}(\boldsymbol{s}_0, t_0) = \sum_{i=1}^{n} \lambda_i Z(\boldsymbol{s}_i, t_i) \tag{1}$$

where $\hat{Z}(\boldsymbol{s}_0, t_0)$ is the value at a location and time that is not observed, λ_i is a spatio-temporal kriging weights, and $Z(\boldsymbol{s}_i, t_i)$ is the value at an observed location and time. The weights in the spatio-temporal ordinary kriging model, which assumes an unknown mean and stationary data, can be determined using equation (2).

$$\begin{pmatrix} \lambda_1 \\ \vdots \\ \lambda_n \\ \alpha \end{pmatrix} = \begin{pmatrix} \gamma(\boldsymbol{s}_1 - \boldsymbol{s}_1, t_1 - t_1) & \cdots & \gamma(\boldsymbol{s}_1 - \boldsymbol{s}_n, t_1 - t_n) & 1 \\ \vdots & \ddots & \vdots & \vdots \\ \gamma(\boldsymbol{s}_n - \boldsymbol{s}_1, t_n - t_1) & \cdots & \gamma(\boldsymbol{s}_n - \boldsymbol{s}_n, t_n - t_n) & 1 \\ 1 & \cdots & 1 & 0 \end{pmatrix}^{-1} \begin{pmatrix} \gamma(\boldsymbol{s}_1 - \boldsymbol{s}_0, t_1 - t_0) \\ \vdots \\ \gamma(\boldsymbol{s}_n - \boldsymbol{s}_0, t_n - t_0) \\ 1 \end{pmatrix} \tag{2}$$

where n represents the number of spatial points in D, t represents the number of time, $\gamma(\boldsymbol{s}_i - \boldsymbol{s}_j, t_i - t_j)$ represents the semivariogram between two observed spatio-temporal data, and $\gamma(\boldsymbol{s}_i - \boldsymbol{s}_0, t_i - t_0)$ represents the semivariogram between observed $(\boldsymbol{s}_i, t_i)$ and the unobserved $(\boldsymbol{s}_0, t_0)$ data.

B. Stationary Data

Stasionary means that the data depend only on the spatial and temporal lags, it does not depend on the specific locations $\boldsymbol{s}_i$ and $\boldsymbol{s}_j$ or the specific times t_i and t_j. The non-stationarity of spatio-temporal data can be checked by semivariogram so that trends or patterns in the data can be seen in both spatial and temporal terms [12].

1) Stationarity in spatial data

   Spatial non-stationarity occurs when the data depend on their longitude and latitude. The existence of spatial trends can be observed through visualization of data plots against longitude and latitude for each time step [13]. To verify the presence of a trend in the plot, regression analysis can be performed against longitude and latitude for each time step. Spatial non-stationarity can be addressed using the Box-Cox transformation [14]. Data needs to be transformed if $\lambda \neq 1$ or if it is not within the 95% confidence interval.

2) Stationarity in temporal data

   This stationarity test is only performed on the temporal aspect. The test that can be used to check the non-stationarity of panel data is the Im-Pesaran-Shin (IPS) unit root test. The IPS statistic is calculated based on the average value of the Dickey-Fuller statistic for the n panel units [15]. The expected value and standard deviation for DF_{bar} are provided by Im et al. [16]. If the data is not stationary, differencing ($\Delta Z_t = Z_t - Z_{t-1}$) can be performed.

C. Empirical Spatio-Temporal Semivariogram

The semivariogram estimate obtained by the moments' method was given by equation (3) [17].

$$\hat{\gamma}\big(\boldsymbol{h}(l), u(k)\big) = \frac{1}{2\#N\big(\boldsymbol{h}(l), u(k)\big)} \sum_{(\boldsymbol{s}_i, t_i), (\boldsymbol{s}_j, t_j) \in N\big(\boldsymbol{h}(l), u(k)\big)} \Big(Z(\boldsymbol{s}_i, t_i) - Z\big(\boldsymbol{s}_j, t_j\big)\Big)^2 \tag{3}$$

where, $N\big(\boldsymbol{h}(l), u(k)\big) = \big\{(\boldsymbol{s}_i, t_i)\big(\boldsymbol{s}_j, t_j\big) : \boldsymbol{s}_i - \boldsymbol{s}_j \in T\big(\boldsymbol{h}(l)\big), t_i - t_j \in T\big(u(k)\big)\big\}$, $\mathrm{T}\big(\boldsymbol{h}(l)\big)$ is the tolerance area in $\mathbb{R}^d$ around $\boldsymbol{h}(l)$ and $\mathrm{T}\big(u(k)\big)$ is the tolerance area in $\mathbb{R}$ around $u(k)$. $\#N\big(\boldsymbol{h}(l), u(k)\big)$ represents the number of distinct elements in $N\big(\boldsymbol{h}(l), u(k)\big)$, with $l = 1,2 \dots, L$ and $k = 1,2, \dots, K$.

D. Theoretical Spatial and Temporal Semivariogram

For each dimension, a semivariogram model is identified. Some common ones for precipitation cases are exponential and gaussian models. In the spatial component, which uses distance $\boldsymbol{h}$, the equation model is as follows.

1) Exponential model

$$\gamma(|\boldsymbol{h}|) = c_0 + c\left\{1 - exp\left(-\frac{|\boldsymbol{h}|}{a}\right)\right\} \quad (4)$$

2) Gaussian model

$$\gamma(|\boldsymbol{h}|) = c_0 + c\left\{1 - exp\left(-\frac{|\boldsymbol{h}|^2}{a^2}\right)\right\} \quad (5)$$

In these formulations, $\gamma(|\boldsymbol{h}|)$ denotes the semivariance at a given lag or distance h, representing the average dissimilarity between data points separated by that lag. The parameter c_0 is the nugget, which captures spatially uncorrelated variance often due to measurement error or microscale variability. The parameter c reflects the structured variability or the proportion of variance explained by spatial autocorrelation. The range (a) defines the maximum distance at which observations remain correlated; beyond this distance, spatial dependence becomes negligible. The sill, given by $c_0 + c$, indicates the semivariance value at which the variogram plateaus, meaning that further separation between points does not increase variance. These models are equally applicable to the temporal dimension by replacing the spatial lag h with temporal lag u, allowing the analysis of temporal dependencies in addition to spatial ones.

E. Theoretical Spatio-Temporal Semivariogram

1) Product model or separable model
   Assumes that the spatio-temporal semivariogram is given by equation (6).

$$\gamma(\boldsymbol{h}, u) = C_t(\boldsymbol{0})\gamma_s(\boldsymbol{h}) + C_s(\boldsymbol{0})\gamma_t(u) - \gamma_s(\boldsymbol{h})\gamma_t(u)), (\boldsymbol{h}, u) \in \mathbb{R}^d \times \mathbb{R} \quad (6)$$

2) Product-sum model
   The semivariogram for the product-sum model is shown in equation (7).

$$\gamma(\boldsymbol{h}, u) = \big(k_2 + k_1 C_t(\boldsymbol{0})\big)\gamma_s(\boldsymbol{h}) + \big(k_3 + k_1 C_s(\boldsymbol{0})\big)\gamma_t(u) - k_1\gamma_s(\boldsymbol{h})\gamma_t(u) \quad (7)$$

   where, C_s and C_t is a covariance function, γ_s and γ_t is the semivariogram, $k_1, k_2, k_3 > 0$ and $k_1 + k_2 + k_3 > 0$ is a constant that validate the model. $C_s(\boldsymbol{0})$ is a sill from γ_s and $C_t(\boldsymbol{0})$ is a sill from γ_t.

3) Metric model
   The metric model is a model whose semivariogram function is shown in equation (8).

$$\gamma(\boldsymbol{h}, u) = \gamma\sqrt{\|\boldsymbol{h}\|^2 + (k.|u|)^2}, \quad (\boldsymbol{h}, u) \in \mathbb{R}^d \times \mathbb{R}, c > 0 \quad (8)$$

   where $\|\boldsymbol{h}\| + c|u|$ is the distance on $\mathbb{R}^d \times \mathbb{R}$ and c is a positive contant.

4) Sum-metric model
   In semivarogram terms, the combined metric-sum model is given by equation (9).

$$\gamma(\boldsymbol{h}, u) = \gamma_s(\boldsymbol{h}) + \gamma_t(u) + \gamma\sqrt{\|\boldsymbol{h}\|^2 + (k.|u|)^2}, (\boldsymbol{h}, u) \in \mathbb{R}^d \times \mathbb{R}, c > 0 \quad (9)$$

5) Simple sum-metric model
   The simple sum-metric model follows a separable form with the semivariogram function shown in equation (18).

$$\gamma(\boldsymbol{h}, u) = c_0 + \gamma_s(\boldsymbol{h}) + \gamma_t(u) + \gamma\sqrt{\|\boldsymbol{h}\|^2 + (k.|u|)^2}, (\boldsymbol{h}, u) \in \mathbb{R}^d \times \mathbb{R}, c > 0 \quad (10)$$

F. Cross Validation

The best model is determined based on the resulting forecast error value. The smaller the forecast error produced by a model, the better it is for predicting. One criterion for evaluating forecast error is the RMSE (Root Mean Square Error), calculated using the formula in equation (19) [18].

$$RMSE: \sqrt{\sum_{l=1}^{L}\sum_{k=1}^{K}\frac{\left(\gamma(\boldsymbol{h}(l),u(k))-\hat{\gamma}(\boldsymbol{h}(l),u(k))\right)^2}{n}} \quad (11)$$

with $\gamma(\boldsymbol{h}(l),u(k))$ is empirical semivariogram value at spatial distance $\boldsymbol{h}(l)$ and temporal distance $u(k)$, $\boldsymbol{h}(l)$ is spatial distance of size l, $u(k)$ is temporal distance of size k, and n = total number of spatio-temporal pairs in the corresponding lags.

G. Precipitation

Precipitation is the amount of rain that falls in an area over a specific period [19]. It is the hydrological cycle's most important driving force [20]. Precipitation exhibits a high causal correlation both spatially and temporally [21]. The most obvious results of changes in the Earth's climate system are variations in precipitation on regional and temporal scales [22]. Sea surface temperature has a significant influence on the amount of precipitation, especially when considering wind direction, season, and topography [23], [24]. This means that the closer an area is to the sea, the more water vapor is available for cloud formation and precipitation. During the rainy season, coastal areas can experience a significant increase in precipitation due to increased sea surface temperatures, which raise the rate of evaporation, resulting in more water vapor in the atmosphere. However, in the dry season, precipitation in coastal areas can be very low because evaporation decreases and clouds tend to move toward land or mountains. Therefore, precipitation on the coast tends to be more volatile than in hilly areas [25]. Based on topographic variations, the higher the elevation, the higher the potential for precipitation, making rain events more likely [26]. According to BMKG, monthly precipitation is categorized into four levels: low (0–100 mm), medium (100–300 mm), high (300–500 mm), and very high (>500 mm) [19].

III. METHODOLOGY

The data used in this study are secondary data obtained from the Meteorology, Climatology, and Geophysics Agency (BMKG) of Samarinda. The variables used are longitude, latitude, and total monthly precipitation at seven precipitation observation posts that are spread across Berau, East Kutai, Kutai Kartanegara, Samarinda, Balikpapan, and West Kutai from January 2021 to December 2023. The method applied in this study is spatio-temporal kriging, executed through the following analytical steps.

1. Ploting precipitation data to understand its distribution and characteristics.
2. Testing the stationarity of the data spatially by forming a regression
3. Performing a Box-cox transformation if the data is found to be non spatially stationary
4. Testing the stationarity of the data temporally using the IPS test
5. Applying differencing to the temporal aspect if it is not temporally stationary
6. Constructing the empirical spatio-temporal semivariogram using equation (3)
7. Developing the theoretical spatio-temporal semivariogram for all models using equations (4) to (10)
8. Fitting the best semivariogram model by comparing the resulting RMSE and selecting the model with the smallest value using equation (11).
9. Performing spatio-temporal kriging interpolation based on equation (1).
10. Mapping the interpolation results.

IV. RESULTS AND DISCUSSIONS

A. Descriptive Statistics

The precipitation at each spatial point and time step shows that the distribution pattern of precipitation is random and does not depend on specific locations (longitude and latitude). This indicates that, visually, there is no significant trend in the data, suggesting that the data are spatially stationary. This is illustrated in Figure 1, which displays precipitation plots based on longitude (easting) and latitude (northing) separately, using samples from October to December 2023. Visualization to determine spatial stationarity can also be observed from the empirical semivariogram in Figure 3, which shows that the semivariogram does not exhibit a spatial trend at any time. This indicates that the precipitation phenomenon in East Kalimantan, from a spatial perspective, is influenced solely by distance rather than the specific longitude and latitude of a location. Therefore, it can be concluded that precipitation in East Kalimantan is spatially stationary. The absence of easting and northing on precipitation is further supported by the regression results, which indicate that for the entire observation period, easting and northing have no significant effect. This is evidenced by the p-value of the easting and northing parameters, which is more than 0.05. Based on the regression results and using a significance level (α) of 0.05, it concluded that the data is spatially stationary, meaning no data transformation is necessary. A significance level of 0.05 is used as an acceptable error threshold when rejecting the null hypothesis. With a

p-value greater than 0.05, it suggests that the probability of error from rejecting the null hypothesis exceeds the specified significance level (0.05), implying that the error is too large if concluding that the alternative hypothesis (which posits a significant effect of the parameter) is true. Conversely, if the null hypothesis is accepted, the error is small, suggesting that the parameter has no effect.

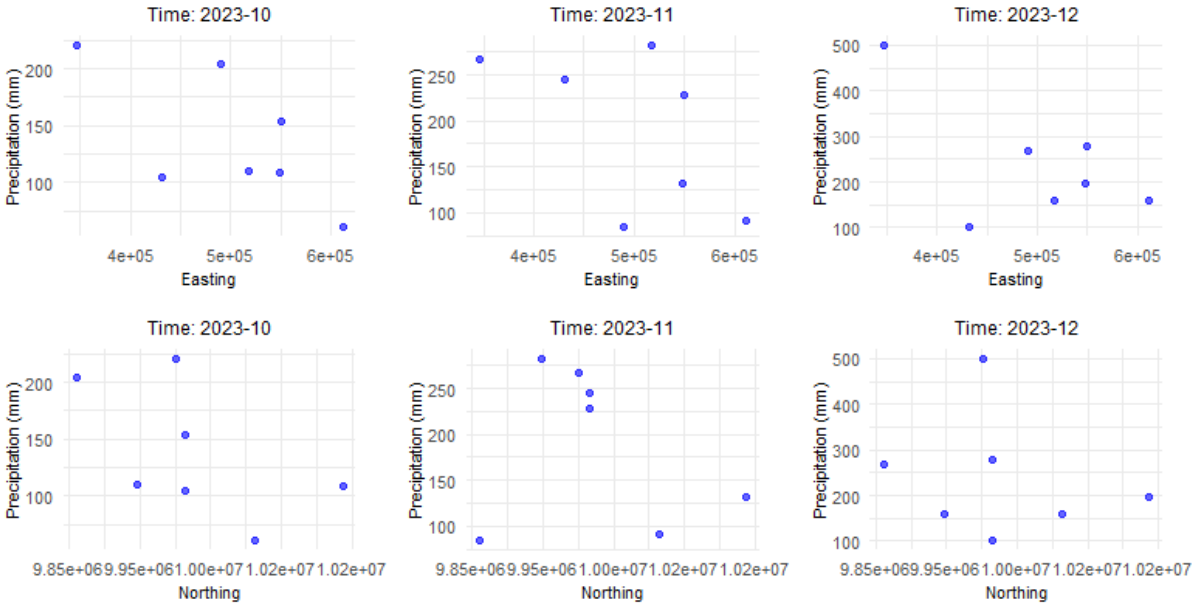

Figure 1 Precipitation based on longitude (easting) and latitude (northing)

Precipitation over time for each precipitation observation post, as reflected in Figure 2, shows that the data is temporally stationary because the overall precipitation exhibits a constant average and variation over time. With an average Dickey Fuller statistic of -4.80, where the expected value and standard deviation for DF_{bar} provided by Im et al. are -1.524 and 0.780, respectively, the IPS test statistic is calculated as -9.742 with a p-value of 0. This indicates that the null hypotesis (H_0), which states that the data is not stationary, is rejected. In other words, the precipitation observation data in East Kalimantan is temporally stationary. Therefore, the precipitation data in East Kalimantan is stationary in both spatial and temporal aspects. With the average precipitation unknown, the spatio-temporal ordinary kriging model is the most appropriate to use. Based on the precipitation plot in Figure 2, it is known that the Long Iram precipitation post records higher precipitation than other observation locations. This higher precipitation may result from a combination of geographical and vegetation factors. Long Iram is situated in an area with higher topography than other regions, leading to orographic phenomena and more frequent formation of active convective clouds, which trigger higher precipitation.

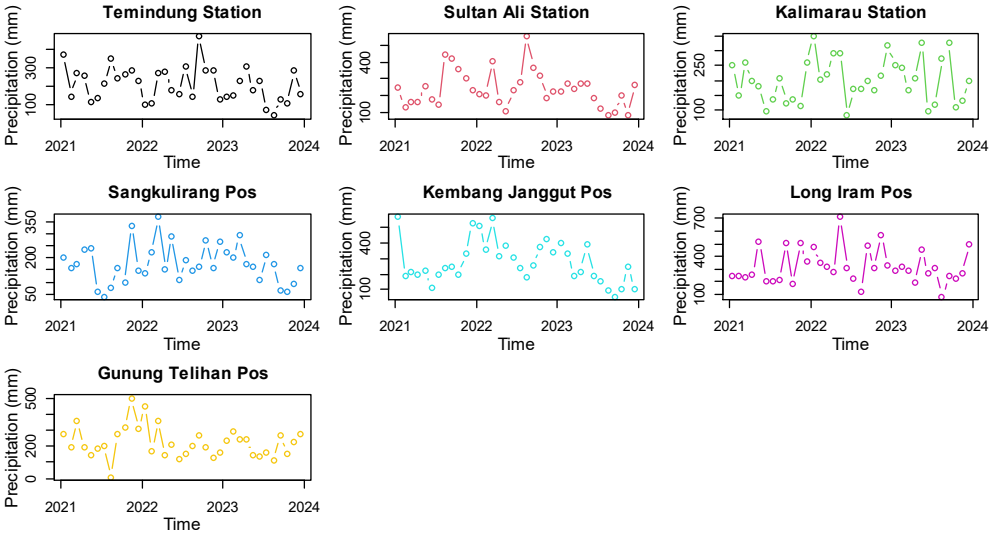

Figure 2 Precipitation for each observation point

B. Theoretical Spatio-Temporal Semivariogram

Spatial-temporal kriging modeling uses a semivariogram to account for the variability between data points, as well as the relationships between spatial, temporal, and joint spatio-temporal distances. The results of matching various theoretical models to the empirical semivariogram produce the RMSE presented in Table 1. The simple sum-metric model, where the spatial semivariogram follows an exponential model while temporal and joint semivariogram models follow a gaussian model, is identified as the best spatio-temporal semivariogram model, producing the lowest RMSE of 2493.687.

Table 1 RMSE Spatio-Temporal Semivariogram Model

RMSE Spatio-Temporal Model	Joint Model	Spatial and Temporal Semivariogram Model				Joint Model	
		Exp+Exp	Exp+Gau	Gau+Exp	Gau+Gau	Exp	Gau
Separable	·	2518.211	2518.209	2520.403	2520.337	·	·
Product-sum	·	3104.620	3279.656	2983.741	2868.631	·	·
Metric	·	·	·	·	·	2523.381	2523.475
Sum-metric	Exp	2522.348	2522.350	2522.352	2522.349	·	·
	Gau	2502.212	2501.695	2501.505	2493.735	·	·
Simple sum-metric	Exp	2523.751	2523.756	2523.756	2523.756	·	·
	Gau	2493.839	2493.687	2493.738	2493.721	·	·

*Exp+Gau means spatial semivariogram follows an exponential model and the temporal semivariogram follows a gaussian model

The results of the fit semivariogram model, simple sum-metric, produce parameters on the spatial component in the form of partial sill of 1664.27 and a range of 56,414.54, parameters on the temporal component in the form of partial sill of 15,306.94 and a range of 16,599.69, parameters on the joint component in the form of partial sill of 3857.67 and a range of 183,974.10, nugget model of 7317.03, and anisotropy correction of 84,458.50, then the following model can be made.

$$\gamma(\boldsymbol{h},u) = 7317.03 + \gamma_s(\boldsymbol{h}) + \gamma_t(\boldsymbol{u}) + \gamma\left(\sqrt{\|\boldsymbol{h}\|^2 + (84{,}458.50|u|)^2}\right), (\boldsymbol{h},u) \in \mathbb{R}^d \times \mathbb{R}, c > 0$$

with,

$$\gamma_s(|\boldsymbol{h}|) = 1664.27\left\{1 - exp\left(-\frac{|\boldsymbol{h}|}{56{,}414.54}\right)\right\}$$

$$\gamma_t(\boldsymbol{u}) = 15{,}306.94\left\{1 - exp\left(-\frac{|h|^2}{16{,}599.69^2}\right)\right\}$$

$$\gamma\left(\sqrt{\|\boldsymbol{h}\|^2 + (84{,}458.50|u|)^2}\right) = 3857.67\left\{1 - exp\left(-\frac{\|\boldsymbol{h}\|^2 + (84{,}458.50|u|)^2}{183{,}974.10^2}\right)\right\}$$

Figure 3 presents the spatio-temporal empirical semivariogram, which illustrates the sample variability of precipitation phenomena in East Kalimantan, compared to the simple sum-metric semivariogram, identified as the best-fitting spatio-temporal semivariogram.

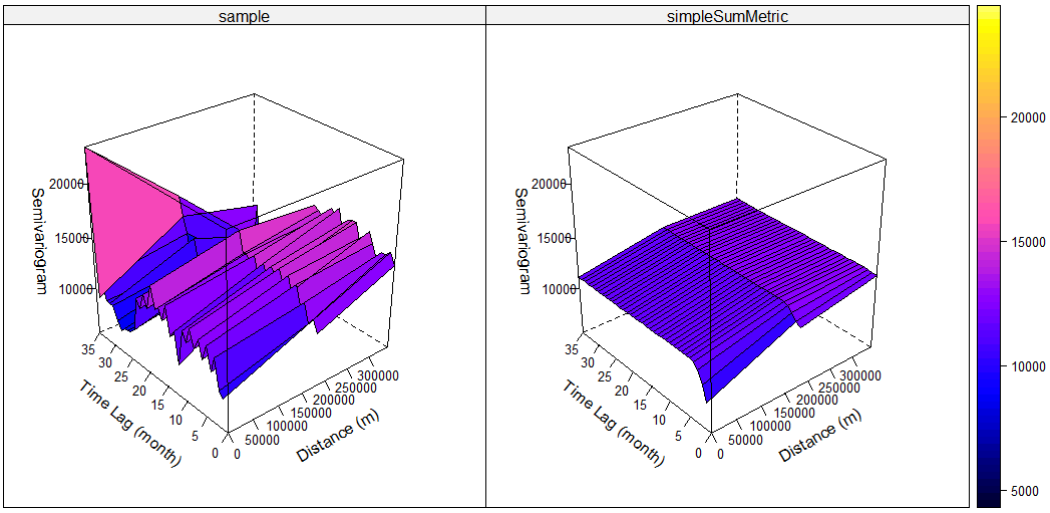

Figure 3 Empirical semivariogram and the best fitting (simple sum-metric) semivariogram

In the spatial component, the partial sill of 1664.27 represents pure spatial structural variance after excluding the nugget effect (random noise). The range of 56,414.54 meters (56.41 km) signifies the maximum spatial correlation distance. Beyond this distance, two locations are considered uncorrelated. In the temporal component, the partial sill of 15,306.94 indicates the pure temporal structural variance after excluding the nugget effect, while the range of 16,599.69 months suggests that the correlation between precipitation measurements at two different times diminishes significantly after this time interval. The same interpretation is applied to the joint component. The nugget model of 7317.03 implies variations that the semivariogram model cannot explain at zero distance, often attributed to measurement errors. The addition of nuggets and partial sills for either spatial or temporal components shows maximum variance when spatial or

temporal correlations are still present. Anisotropy correction is an adjustment made to handle differences in spatial or temporal correlation so that they have the same scale. Anisotropy correction of 84,458.50 suggests that one temporal unit is equivalent to a spatial distance of 84.46 km, addressing the scale disparity between spatial and temporal correlations.

C. Interpolation

Based on the interpolation visualization shown in the plot in Figure 4, the Long Iram precipitation post exhibits higher precipitation compared to other areas in East Kalimantan. The recorded precipitation at Long Iram precipitation post located in West Kutai Regency has the potential to spread to the surrounding areas. The interpolation visualization contour in Figure 4 shows that the entire area of West Kutai Regency experiences a high precipitation interval, with the highest precipitation in Long Iram District and its surrounding areas, including Long Hubung District in Mahakam Ulu Regency and parts of Kembang Janggut District in Kutai Kartanegara Regency. The phenomenon of higher precipitation in West Kutai Regency compared to coastal areas aligns with the theory that higher altitudes experience more precipitation due to the orographic effect. When humid air is compelled to ascend to high elevations, the air then cools and condenses, resulting in the formation of clouds and precipitation. Although Balikpapan's altitude is higher than West Kutai's, the latter experiences more precipitation due to its mountainous terrain and higher hills. These geographical features enhance the orographic effect, where moist air carried by the wind rises upon meeting the mountains, cools, and condenses, resulting in increased precipitation. In contrast, despite its higher altitude, Balikpapan lacks the complex topography necessary to intensify this process significantly.

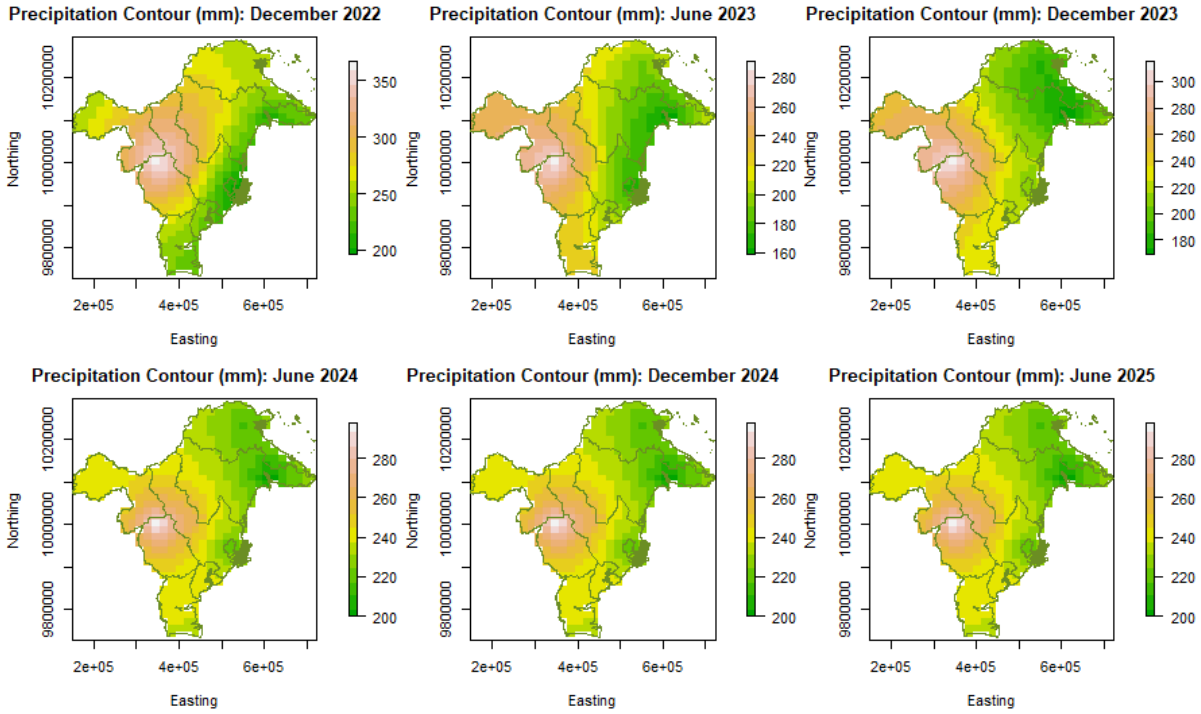

Figure 4 Spatio-temporal kriging interpolation contour

In December 2022 to December 2023, average precipitation in the West Kutai and Mahakam Ulu ranged from 300 to 370 mm per month, classifying it as high precipitation, whereas other areas experienced medium precipitation (200–300 mm per month). Interpolation for June 2025 shows all areas in East Kalimantan falling into the medium category, with precipitation between 200 and 300 mm per month. Penajam Paser Utara, as the relocation district for IKN, shows medium precipitation with an average precipitation of 240 mm per month. Based on the interpolation results in the form of contours shown in Figure 4 above, there is no significant change in precipitation patterns with an average amount of precipitation in the East Kalimantan region of 200 to 300 mm per month. Spatially, precipitation patterns are stable over time, with the highest precipitation in Long Iram, West Kutai and the lowest in Sangkulirang, East Kutai. Having higher interval precipitation than other areas, the West Kutai area requires special attention for flood hazards mitigation because it is identified as a flood-prone area so further mitigation efforts need to be made. In addition, water conservation needs to be carried out in the area such as by improving water absorption, which can be done through effective drainage management, reforestation, and tree planting.

V. CONCLUSIONS AND SUGGESTIONS

The simple sum-metric with an exponential spatial semivariogram and gaussian temporal and joint semivariograms achieves an RMSE of 2493.687, making it the most suitable spatio-temporal semivariogram model for capturing precipitation variability in East Kalimantan both in spatial and temporal dimensions. Mapping results indicate that until June 2025, West Kutai remains flood-prone areas because it has precipitation that is included in the medium to high precipitation category and can spread to the surrounding areas, while other areas have precipitation in the medium category. Special attention is needed for water conservation and flood disaster mitigation by related institutions to minimize flood risk and manage rainwater effectively for community welfare.

REFERENCES

[1] Z. Zhu, D. B. Wright, and G. Yu, "The Impact of Rainfall Space-Time Structure in Flood Frequency Analysis," *Water Resour Res*, vol. 54, no. 11, pp. 8983–8998, Nov. 2018, doi: 10.1029/2018WR023550.

[2] T. W. Sudinda, "Pemanfaatan Air Hujan untuk Memenuhi Kebutuhan Air Baku Jangka Panjang Ibu Kota Negara," *Construction Engineering and Sustainable Development*, vol. 3, no. 1, pp. 1–48, Jun. 2020, Accessed: Mar. 09, 2025. [Online]. Available: https://www.e-journal.trisakti.ac.id/index.php/sipil/article/view/13654

[3] R. Olanrewaju, B. Ekiotuasinghan, and G. Akpan, "Analysis of rain fall pattern and flood incidences in Warri metropolis, Nigeria," *Geography, Environment, Sustainability*, vol. 10, no. 4, pp. 83–97, 2017, doi: 10.24057/2071-9388-2017-10-4-83-97.

[4] Y. Chen, A. Paschalis, L. P. Wang, and C. Onof, "Can we estimate flood frequency with point-process spatial-temporal rainfall models?," *J Hydrol (Amst)*, vol. 600, Sep. 2021, doi: 10.1016/j.jhydrol.2021.126667.

[5] P. Liu and Y. K. Tung, "Spatial interpolation of rain-field dynamic time-space evolution based on radar rainfall data," *Hydrology Research*, vol. 51, no. 3, pp. 521–540, Jun. 2020, doi: 10.2166/nh.2020.115.

[6] A. Verdin, C. Funk, B. Rajagopalan, and W. Kleiber, "Kriging and local polynomial methods for blending satellite-derived and gauge precipitation estimates to support hydrologic early warning systems," *IEEE Transactions on Geoscience and Remote Sensing*, vol. 54, no. 5, pp. 2552–2562, May 2016, doi: 10.1109/TGRS.2015.2502956.

[7] A. S. Abdullah *et al.*, "Implementation of Generalized Space Time Autoregressive (GSTAR)-Kriging model for predicting rainfall data at unobserved locations in West Java," *Applied Mathematics and Information Sciences*, vol. 12, no. 3, pp. 607–615, May 2018, doi: 10.18576/amis/120316.

[8] E. A. Varouchakis, D. T. Hristopulos, G. P. Karatzas, G. A. C. Perez, and V. Diaz, "Spatiotemporal geostatistical analysis of precipitation combining ground and satellite observations," *Hydrology Research*, vol. 52, no. 3, pp. 804–820, Jun. 2021, doi: 10.2166/nh.2021.160.

[9] N. B. Raja, O. Aydin, N. Türkoğlu, and I. Çiçek, "Space-time kriging of precipitation variability in Turkey for the period 1976–2010," *Theor Appl Climatol*, vol. 129, no. 1–2, pp. 293–304, Jul. 2017, doi: 10.1007/s00704-016-1788-8.

[10] J. R. P. De Carvalho, A. M. Nakai, and J. E. B. A. Monteiro, "Modelagem espaço temporal para imputação de dados para séries de precipitação diária em zonas homogêneas," *Revista Brasileira de Meteorologia*, vol. 31, no. 2, pp. 196–201, Apr. 2016, doi: 10.1590/0102-778631220150025.

[11] J.-M. Montero, G. Fernández-Avilés, and J. Mateu, *Spatial and Spatio-Temporal Geostatistical Modeling and Kriging*, 1st ed. United Kingdom: John Wiley & Sons, Ltd, 2015. doi: 10.1002/9781118762387.

[12] L. Shand and B. Li, "Modeling nonstationarity in space and time," *Biometrics*, vol. 73, no. 3, pp. 759–768, Sep. 2017, doi: 10.1111/biom.12656.

[13] N. N. Rohma, H. Pramoedyo, and S. Astutik, "Perbandingan Pendugaan Metode Ordinary Kriging dan Metode Ordinary Kriging dengan Teknik Jackknife," *MAp (Mathematics and Applications) Journal*, vol. 2, no. 4, pp. 101–111, 2023, doi: https://doi.org/10.15548/map.v4i2.4736.

[14] J. D. Cryer and K.-S. Chan, *Time Series Analysis with Applications in R*, 2nd ed. Iowa: Springer, 2008. doi: https://doi.org/10.1007/978-0-387-75959-3.

[15] V. Murthy and A. Okunade, "Is the health care price inflation in US urban areas stationary?: Evidence from panel unit root tests," *Journal of Economics, Finance and Administrative Science*, vol. 23, no. 44, pp. 77–94, Jun. 2018, doi: 10.1108/JEFAS-02-2017-0043.

[16] K. S. Im, M. H. Pesaran, and Y. Shin, "Testing for unit roots in heterogeneous panels," *J Econom*, vol. 115, no. 1, pp. 53–74, Jul. 2003, doi: 10.1016/S0304-4076(03)00092-7.

[17] X. Yang, Y. Yang, K. Li, and R. Wu, "Estimation and characterization of annual precipitation based on spatiotemporal kriging in the Huanghuaihai basin of China during 1956–2016," *Stochastic Environmental Research and Risk Assessment*, vol. 34, no. 9, pp. 1407–1420, Sep. 2020, doi: 10.1007/s00477-019-01757-0.

[18] N. Islam, A. Kashem, P. Das, M. N. Ali, and S. Paul, "Prediction of high-performance concrete compressive strength using deep learning techniques," *Asian Journal of Civil Engineering*, vol. 25, no. 1, pp. 327–341, Jan. 2024, doi: 10.1007/s42107-023-00778-z.

[19] BMKG, "Pandangan Iklim 2025," Jakarta, Oct. 2024.

[20] O. M. Katipoğlu, "Spatial analysis of seasonal precipitation using various interpolation methods in the Euphrates basin, Turkey," *Acta Geophysica*, vol. 70, no. 2, pp. 859–878, Apr. 2022, doi: 10.1007/s11600-022-00756-0.

[21] W. Zhang, D. Liu, S. Zheng, S. Liu, H. A. Loáiciga, and W. Li, "Regional precipitation model based on geographically and temporally weighted regression kriging," *Remote Sens (Basel)*, vol. 12, no. 16, pp. 1–19, Aug. 2020, doi: 10.3390/RS12162547.

[22] B. O. Ayugi, W. Yan, W. Shanghai, J. Tong, W. Wen, and D. Chepkemoi, "Analysis of Spatial and Temporal Patterns of Rainfall Variations over Kenya," *Journal of Environment and Earth Science*, vol. 6, no. 11, pp. 69–83, 2016, [Online]. Available: www.iiste.org

[23] M. A. Pertiwi, S. Kahar, B. Sasmito, and S. Marpaung, "Analisis Korelasi Suhu Permukaan Laut Terhadap Curah Hujan dengan Metode Penginderaan Jauh Tahun 2012-2013 (Studi Kasus : Kota Semarang)," *Jurnal Geodesi Undip Januari*, vol. 4, no. 1, pp. 61–71, 2015, doi: https://doi.org/10.14710/jgundip.2015.7639.

[24] I. B. A. P. Adiguna, I. W. Nuarsa, and N. L. P. R. Puspitha, "Pengaruh Suhu Permukaan Laut terhadap Curah Hujan di Pulau Bali Tahun 2009-2018," *Journal of Marine and Aquatic Sciences*, vol. 7, no. 2, p. 214, Dec. 2021, doi: 10.24843/jmas.2021.v07.i02.p10.

[25] M. F. Islami, N. F. T, N. Falah, F. Khairunnisa, and N. A. Jamal, "Analisis Karakteristik Perbandingan Curah Hujan Wilayah Pesisir dan Wilayah Perbukitan Kota Makassar," *LaGeografia*, vol. 22, no. 2, p. 196, Feb. 2024, doi: 10.35580/lageografia.v22i2.59403.

[26] R. Tresnawati and Rosyidah, "Validation of Monthly Rainfall Prediction Taken from the Output of Canonical Correlation Analysis using Area Topographical Scenarios in Centra Java Province," *Jurnal Meteorologi dan Geofisika*, vol. 20, no. 1, pp. 1–12, May 2019, [Online]. Available: http://www.cpc.ncep.noaa.gov/